nature photonics

REVIEW ARTICLE

PUBLISHED ONLINE: 4 DECEMBER 2011 | DOI: 10.1038/NPHOTON.2011.285

Surface plasmon–polariton amplifiers and lasers

Pierre Berini* and Israel De Leon

Amplifiers and lasers based on surface plasmon–polaritons (SPPs) have been studied for around three decades. Research in this area has experienced particularly significant growth over the past decade, resulting in the achievement of several important milestones. Convincing demonstrations of SPP amplification and lasing have been reported for various systems involving single-interface, long-range, short-range and resonant SPPs. Diverse metallic structures such as planes, films, stripes, wires and particles (some on the nanoscale) have been integrated with gain materials. Although the prospects for SPP amplifiers and lasers are bright, the field is embryonic, and much remains to be explored and improved. This Review discusses this rapidly progressing area and summarizes the most important progress achieved so far. Research directions that warrant further investigation are also suggested.

A surface plasmon–polariton (SPP) is a transverse magnetic (TM)-polarized optical surface wave that propagates, for example, along a flat metal–dielectric interface, typically at visible or infrared wavelengths[1]. It is a coupled excitation comprising a charge density wave in the metal and electromagnetic fields that peaks at the interface and decay exponentially into both media (Box 1). Other metal structures supporting SPPs include thin metal films and stripes, metal nanoparticles of various shapes and sizes, and holes, slits, gaps, grooves or corrugations in metal films[1]. SPPs exhibit a range of interesting and useful properties, such as energy asymptotes in dispersion curves, resonances, field enhancement and localization, high surface and bulk sensitivities, and subwavelength confinement. Because of these attributes, SPPs have found applications in fields such as spectroscopy[2], nanophotonics[3,4], imaging[5], biosensing[6,7] and circuitry[8].

SPPs dissipate their energy primarily through interaction with the metal. For a metal bounded by an ideal dielectric, loss is caused by free-electron scattering in the metal and, at short enough wavelengths, by absorption via interband transitions (see also the measured optical parameters of metals[9]). These loss mechanisms are fundamental to SPPs. Absorption via interband transitions may be avoided by careful selection of the operating wavelength, but free-electron scattering, which, although can be reduced by improved fabrication techniques, cannot be eliminated altogether. Roughness along the metal interface causes additional loss by scattering SPPs into bulk waves.

Excessive loss limits the scope of SPPs for practical applications. For example, loss limits the SPP propagation length and therefore the depth of its energy asymptote by 'bending back' its dispersion curve[10]. Researchers have proposed loss compensation and amplification approaches that add optical gain to the dielectric(s) bounding the metal. 'Loss compensation' here means that SPP losses are reduced compared with the passive case, whereas 'amplification' means that they are overcompensated. The gain required for amplification depends on the confinement of the SPP. In general, the more confined the SPP, the greater its attenuation and the greater the required gain. This confinement–attenuation trade-off[11,12] (Box 1) does not exist in dielectric waveguides, where the attenuation is negligible for well-fabricated structures.

The quantum optics of SPPs, although intimately related to the topics discussed here, is beyond the scope of this Review. However, a few important points are worth making. First, SPPs satisfy Maxwell's equations and the applicable boundary conditions. Second, they are bosons and therefore satisfy boson commutation rules, even though electrons are collectively involved. Third, SPPs can be energy quantized in the usual way by analogy with a quantum harmonic oscillator incorporating material dispersion[13,14] and absorption[15]. One may then speak of an SPP as gaining or losing a quantum of energy in processes that involve atoms, molecules or continuous media such as spontaneous and stimulated emission/absorption (Box 2). Finally, an SPP's optical density of states can be defined and used in the assessment of, for example, spontaneous emission rates in various structures[16].

The amplification of SPPs sets the foundation for many interesting, useful and compelling applications, which has motivated much of the research on this topic. One envisions, for instance, SPP amplifiers either as stand-alone components or as 'gain blocks' integrated with plasmonic elements[3–5], biosensors[6,7] or circuitry[8] to compensate for losses or otherwise improve performance. Incorporating feedback with SPP amplifiers leads to the realization of SPP oscillators — known as SPP lasers or 'spasers' — which are of great interest in their own right as sources of coherent SPPs. Such applications are achievable with nanoscale structures because SPPs can be confined to deep subwavelength dimensions.

The properties of SPPs, and the rich variety of metallic structures on which they are supported, mean that SPP amplifiers and oscillators are distinct from their conventional counterparts in terms of form and performance. The organization of this Review reflects this diversity: work on single-interface SPPs is covered first, followed by work on metal films, metal clads and variants thereof, and finally by work on nanostructures. The integration of gain with plasmonic metamaterials is also being vigorously pursued, but this topic is beyond the scope of this Review.

Single-interface SPPs

Prism and grating coupling configurations are convenient for exciting SPPs[1]. The Kretschmann configuration consists of a metal film on the base of a high-refractive-index prism, bounded by a low-refractive-index medium on the other side (Fig. 1a). A grating coupler introduces a periodic perturbation of corrugations, bumps or slits to the metal (Fig. 1c). The role of the prism or grating is to increase the in-plane momentum of TM-polarized incident light such that it matches that of the SPP. Several theoretical and experimental studies have been conducted in such configurations[17–30].

School of Electrical Engineering and Computer Science, University of Ottawa, 161 Louis Pasteur St, Ottawa, Ontario K1N 6N5, Canada; Department of Physics, University of Ottawa, 150 Louis Pasteur St, Ottawa, Ontario K1N 6N5, Canada. *e-mail: berini@eecs.uottawa.ca

© 2011 Macmillan Publishers Limited. All rights reserved.

Box 1 | SPPs on planar structures

The simplest SPP waveguide is a single metal–dielectric interface (Fig. B1a). Metals have a negative real part of permittivity and are dispersive[9], which causes the single-interface SPP (SISPP) wavenumber to diverge at a specific wavelength[1]. The photon energy where this occurs is known as the 'energy asymptote'. The properties of an SISPP reach extremes at the asymptote, but losses limit its depth by 'bending back' the dispersion curve to the left of the light line[10]. Table B1 lists the modal characteristics of an SISPP on an Ag–SiO_2 interface at three wavelengths (λ = 360 nm is near the asymptote)[12].

A thin metal film bounded by symmetric dielectrics (Fig. B1b) supports two SPP supermodes created from either symmetric or asymmetric couplings of SISPPs[44]. The symmetric mode, whose attenuation can be much lower than that of an SISPP, is therefore a long-range SPP (LRSPP)[31–33]. This reduced attenuation, however, comes with reduced confinement[11,12]. The asymmetric mode, which behaves oppositely as the metal thickness t decreases, is a short-range SPP (SRSPP). In the Ag–SiO_2 system, the mode power attenuation coefficient (2α) of the LRSPP and SRSPP modes is 0.0012 dB μm^{-1} and 0.45 dB μm^{-1} (2.8 cm^{-1} and 10^3 cm^{-1}), respectively, for t = 20 nm at λ = 1,550 nm, increasing sharply as λ decreases[12]. The reverse structure — a thin dielectric film bounded by metal claddings (Fig. B1c) — also supports SPPs[54]. If the dielectric is thick then many transverse electric (TE) and TM parallel-plate-like modes may be supported, but as $t \to 0$ only the asymmetric SPP is supported. Although this mode can be confined to an arbitrarily small width, its attenuation increases as the thickness is reduced[11,12], which makes it an SRSPP. In the Ag–SiO_2 system, the attenuation of this mode is 0.85 dB μm^{-1} (2×10^3 cm^{-1}) for t = 50 nm at λ = 1,550 nm, but this increases sharply as t and λ decrease[12].

Two-dimensional SPP waveguides provide confinement in the plane transverse to the direction of propagation, which is useful for enabling circuitry[8]. Several popular structures are shown in Fig. B1d–i; many are natural extensions of one-dimensional structures. The dielectric-loaded single-interface waveguide[63,67] (Fig. B1d) and the low-index hybrid waveguide[70,71] (Fig. B1g) allow confinement via a high-refractive-index region. In the former case, the SPP is confined within this region and its attenuation ranges from that of the corresponding SISPP to around ten times this value. In the latter case, the SPP exhibits strong localization to the thin (nanometre-wide) low-refractive-index gap, and its attenuation is bounded by the corresponding low- and high-refractive-index SISPPs. The metal stripe[34] (Fig. B1e) produces lateral confinement by limiting the width of the metal film; although the attenuation of an LRSPP in this design can be around ten times lower than on an infinitely wide film, it remains loosely confined. The gap waveguide[53] (Fig. B1f) resembles rotated metal clads, providing strong SRSPP confinement with an attenuation that is comparable (in magnitude) to that of the metal clads. Wedge and channel waveguides[4] consist of a metal protrusion (Fig. B1h) or a groove in a metal film (Fig. B1i), respectively.

Whether it appears by varying the wavelength or the geometry, the SPP confinement–attenuation trade-off is fundamental; increased confinement leads to greater overlap with the metal(s), which leads to greater attenuation. SPP attenuation therefore spans a very broad range (1–10^5 cm^{-1}), with the most strongly confined modes requiring the greatest material gains for loss compensation, in some cases near or beyond what can be practically achieved.

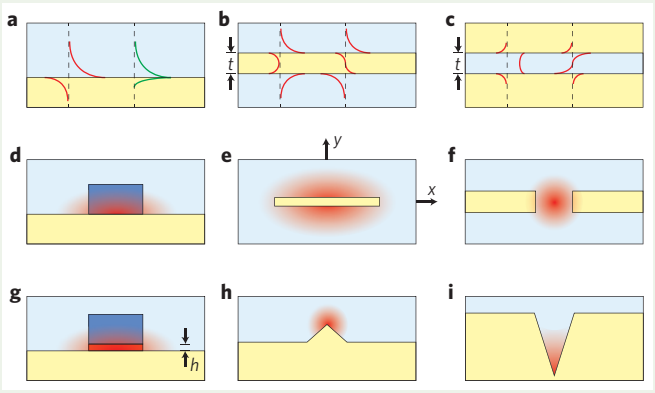

Figure B1 | SPP waveguides. a–c, One-dimensional SPP waveguides. **a**, Metal–dielectric interface, where the SPP mode fields (red, Re{E_y}; green, Re{H_x}) are transverse to the direction of propagation, z. **b**, Metal film sandwiched between two symmetric dielectric clads. **c**, Dielectric film sandwiched between two symmetric metal clads. Also shown are Re{E_y} (red) for the symmetric (left) and asymmetric (right) SPP supermodes. **d–i**, Two-dimensional SPP waveguides. Dielectric-loaded (**d**), metal stripe (**e**), gap (**f**), low-index hybrid (**g**), wedge (**h**) and channel (**i**) waveguides, showing the distribution of the main transverse electric field component of the main symmetric SPP mode supported therein.

Table B1 | Modal characteristics of an SISPP on an Ag–SiO_2 interface at three wavelengths.

λ (nm)	n_{eff}	δ_w (nm)	2α		L (μm)
			(cm^{-1})	(dB μm^{-1})	
360	2.537	44	5×10^5	218	0.02
633	1.565	176	1.6×10^3	0.71	6
1,550	1.457	1,269	1×10^2	0.044	100

$n_{eff} = \beta\lambda/2\pi$, where β is the corresponding propagation constant, δ_w is the 1/e mode field width, α is the field attenuation coefficient and $L = 1/(2\alpha)$ is the 1/e propagation length.

The first study of SPP amplification was reported by Plotz *et al.*[17], who sandwiched an silver film in between a glass prism and a gain medium. Computing the reflectance of the glass–metal interface as a function of the angle of incidence for different gain values showed that the usual reflectance drop that occurs at the SPP excitation angle[1] becomes monotonically shallower as the gain increases, eventually becoming larger than one (known as amplified total reflection). Sudarkin and Demkovic[18], when investigating a similar structure over a broader range of parameters, found that the reflectance does not always increase monotonically with gain, but rather that the SPP field increases and the SPP resonance linewidth narrows monotonically with gain, as expected for SPPs of decreasing attenuation. Sudarkin and Demkovic were the first to suggest a laser based on SPPs.

Avrutsky[21] studied the behaviour of the SPP near its energy asymptote on flat and corrugated (period of around 10 nm) silver surfaces in contact with a gain medium. He found that loss compensation requires a material gain of around 80,000 cm^{-1} and that doing so restores the SPP properties resulting from divergence in the dispersion relation, which are spoiled in the passive

© 2011 Macmillan Publishers Limited. All rights reserved.

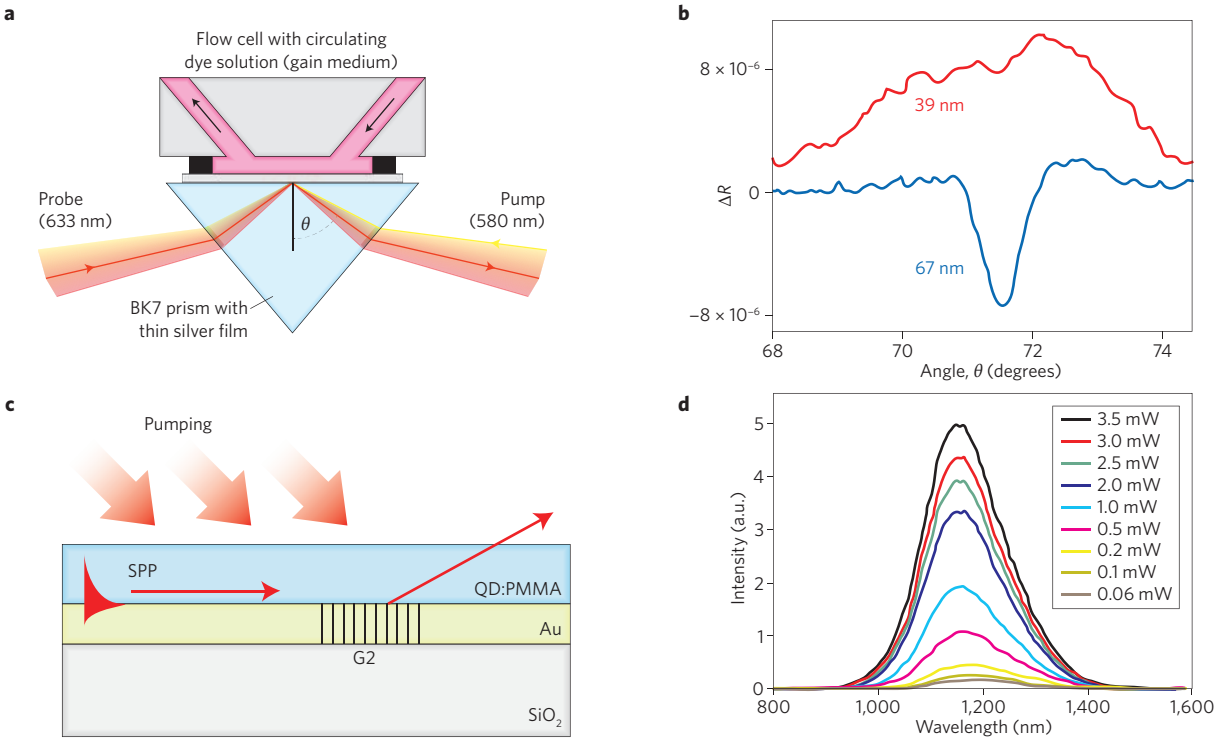

Figure 1 | Stimulated emission of SPPs. a, Dual SPP pump–probe arrangement. **b**, Measured differential reflectance ΔR for cresyl violet ($N = 7 \times 10^{17}$ cm^{-3}) in ethanol as the gain medium, as a function of the probe incidence angle θ. The red and blue curves correspond to silver film thicknesses of 39 nm and 67 nm, respectively. **c**, SPPs propagating through a QD-doped PMMA layer; grating G2 outcouples SPPs to bulk waves. **d**, Measured ASE-SPP spectra as a function of increasing pump irradiance. Figure reproduced with permission from: **a**,**b**, ref. 23, © 2005 APS; **c**,**d**, ref. 29, © 2010 OSA.

case by bend-back[10]. He predicted an extremely low group velocity (~1 km s^{-1}), a large SPP effective index (~29) and strong SPP localization (a few nanometres) on gain-compensated gratings. Achieving such a large material gain poses serious challenges, but it is interesting to note the extreme SPP performance that may be achievable as a result.

Other modelling work includes studies of amplification along metal–semiconductor interfaces[22,25], where lossless SPP propagation has been predicted for silver on InGaAsP that has a material gain of ~1,260 cm^{-1} at a wavelength of $\lambda = 1{,}550$ nm (ref. 22). Parametric SPP amplification on an Ag–$LiNbO_3$ structure has also been investigated[30].

Lasing with SPPs was first demonstrated in quantum cascade lasers operating at far-infrared wavelengths[19,20]. In one device[20], researchers deposited a bimetallic grating on a quantum cascade gain medium to form a distributed-feedback SPP laser emitting at around 17 μm. This device owes its success partly

Box 2 | Dipoles near a metal–dielectric interface

Figure B2 shows several energy-transfer processes that may occur for dipoles near a metal–dielectric interface[40]. Three processes involve SPP quanta for dipoles overlapping spectrally and with SPP electric fields: an excited dipole spontaneously emits an SPP (Fig. B2a); a dipole in the ground state is excited by the absorption of an SPP (Fig. B2b); or an excited dipole is stimulated to emit an SPP clone (Fig. B2c). Other processes involving excited dipoles include the spontaneous creation of electron–hole pairs in the metal through dipole–dipole coupling (for dipoles that are very close) (Fig. B2d) and the spontaneous emission of radiative modes (Fig. B2e). The excitation of radiative modes and electron–hole pairs in the metal corresponds to energy loss. Spontaneously emitted SPPs contribute noise in an amplifier or oscillator application. Amplification requires inversion of the gain medium such that stimulated SPPs dominate over SPP absorption.

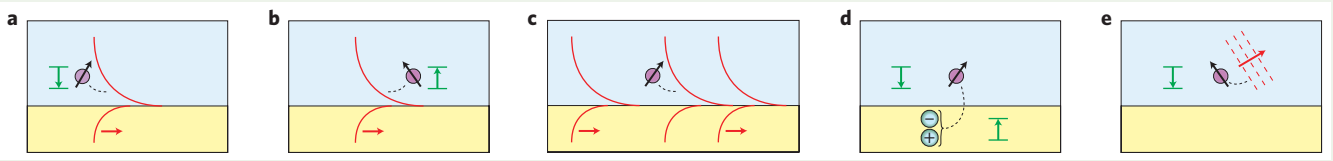

Figure B2 | Optical processes occurring for dipoles (purple) near a single metal–dielectric interface. The magnitude of the transverse electric field component of the SPP involved in the processes (red) is shown along with the associated dipole energy transitions (green). The dotted black curves indicate energy transfer. **a**, Spontaneous emission of SPPs. **b**, Absorption of SPPs. **c**, Stimulated emission of SPPs. **d**, Creation of electron–hole pairs. **e**, Spontaneous emission of radiation.

© 2011 Macmillan Publishers Limited. All rights reserved.

to the low absorption of metals and poor field confinement at such wavelengths.

Seidel *et al.* were the first to observe the stimulated emission of SPPs at optical wavelengths[23]. They used Kretschmann structures comprising 39- and 67-nm-thick silver films on BK7 prisms with the other silver surface being in contact with the gain medium. Rhodamine 101 and cresyl violet, each in ethanol and at a concentration of $N = 7 \times 10^{17}$ cm^{-3}, were used as gain media. TM-polarized light at $\lambda = 633$ nm was used to excite probe SPPs at the silver–dye interface while the dye was excited at $\lambda = 580$ nm (~10 mW) by pump SPPs counter-propagating along the same interface (Fig. 1a). A small differential reflectance ΔR — obtained by comparing cases with and without pumping — was measured as a function of the probe incidence angle θ (Fig. 1b). The non-zero value of ΔR was attributed to the stimulated emission of probe SPPs. For the 39-nm-thick silver film, increased reflectance was noted over the SPP excitation angle, which is in qualitative agreement with theory[17]. For the 67-nm-thick silver film, the reflectance dip was seen to narrow and deepen, which is also in qualitative agreement with theory[18].

Noginov *et al.*[24] investigated a structure similar to that of the Kretschmann configuration, but with the gain medium comprising a 10-μm-thick layer of poly(methyl methacrylate) (PMMA) highly doped ($N = 2.2 \times 10^{22}$ cm^{-3}) with rhodamine 6G (R6G). They pumped the structure strongly from behind at $\lambda = 532$ nm (~18 mJ pulses, ~10 ns duration) and excited probe SPPs via the prism at $\lambda = 594$ nm. They measured an increase in reflectance at the SPP excitation angle due to the stimulated emission of SPPs and estimated an SPP loss reduction of 35% and a material gain of around 420 cm^{-1}. In a subsequent study[26] involving a thinner gain layer (~3 μm), the researchers measured the fluorescence decoupled from the prism during pumping in the absence of the probe and observed characteristics that they attributed to the amplified spontaneous emission of SPPs (ASE-SPPs).

ASE-SPPs were also investigated by Bolger *et al.*[29] using a 100-nm-thick gold film coated with 1 μm of PMMA doped with PbS quantum dots (QDs). They created a grating in the metal film (Fig. 1c) and used it to out-couple SPPs at wavelengths near the QD emission peak. Output spectra narrowed as the pump power increased, which indicates ASE-SPPs (Fig. 1d). They pointed out that significant gain reduction may occur because of ASE-SPPs, and estimated a ~30% increase in SPP propagation length due to stimulated emission.

Long-range SPPs on symmetric metal films

Less material gain is required to amplify long-range SPPs (LRSPPs)[31–34] than single-interface SPPs (SISPPs), which partly justifies their attraction for amplifier and laser applications[35–52]. Nezhad *et al.*[22] calculated that the material gain required for lossless LRSPP propagation in the Ag–InGaAsP system is around 10 times smaller than for SISPPs. By modelling silver stripes on AlGaInAs multiple quantum wells covered by a barrier material, Alam *et al.*[37] predicted that a material gain of ~400 cm^{-1} was required for lossless LRSPP propagation at $\lambda = 1{,}550$ nm. Genov and co-workers investigated silver films bounded by semiconductor multiple quantum wells (InGaAsP[38] and InGaN[42]). Quality factors (Q) of up to 4,000 and threshold gains of around 200 cm^{-1} were predicted at $\lambda = 1{,}400$ nm for LRSPP whispering gallery modes in metal–GaAs microdisk cavities[49].

The lifetime of excited dipoles changes in proximity to metallic structures because they couple to SPPs[16] — an effect that can alter the gain available for amplification[36]. Taking this effect into account, researchers constructed an SPP amplifier model based on a four-level dipolar gain medium[40]. The model incorporates a position-dependent dipole lifetime and an inhomogeneous pump intensity distribution. It was found that if both distributions were neglected, the gain required for lossless propagation would be underestimated

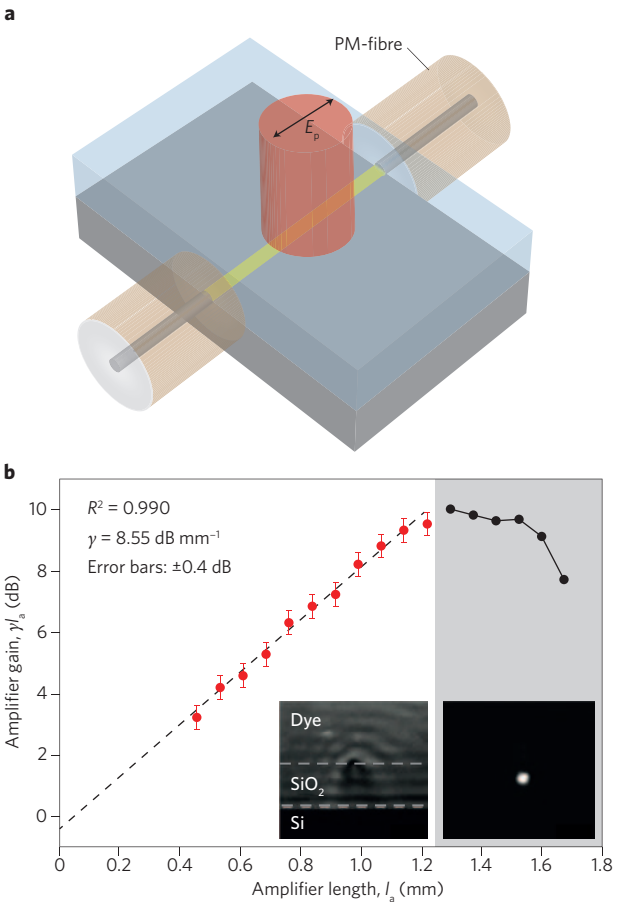

Figure 2 | LRSPP amplifier. a, LRSPP amplifier comprising a gold stripe on SiO_2 (on silicon) covered by a dye gain medium (IR-140). The pump is polarized along the stripe length (E_p) and applied to the top of the structure. End-fire coupled input/output polarization-maintaining (PM) fibres are also shown. **b**, Measured amplifier gain at a probe wavelength of $\lambda = 882$ nm versus amplifier length; the slope of the curve indicates the LPSPP mode power gain ($\gamma = 8.55$ dB mm^{-1}). The inset images show the output of a structure with the pump on but probe off (left), and the pump off but probe on (right). Figure reproduced with permission from: **a**, ref. 46, © 2010 NPG; **b** (left inset), ref. 50, © 2011 APS.

tenfold. Assuming R6G in solvent as the gain medium, lossless LRSPP propagation at $\lambda = 560$ nm was predicted under weak pumping ($\lambda = 532$ nm, ~200 kW cm^{-2}) of a modest dye concentration ($N = 1.8 \times 10^{18}$ cm^{-3}) for a 20-nm-thick silver film covered by the medium[40]. Lossless SISPP propagation was also predicted but for significantly stronger pumping (~3.5 MW cm^{-2}) and a higher dye concentration ($N = 2.4 \times 10^{19}$ cm^{-3})[45].

Several studies involving LRSPPs on corrugated gratings in contact with a gain medium have also been reported. Kawata and co-workers[35,39,48] suggested that a grating supporting LRSPPs would operate as a plasmonic bandgap laser if a gain medium whose peak emission is within the bandgap is introduced. In their concept, standing LRSPP waves would be amplified by stimulated emission and partially out-coupled by the grating to form the laser output. Winter *et al.*[36] pointed out that dipole decay into the asymmetric SPP is substantial and reduces the gain available to the LRSPP. By computing the reflectance and transmittance under normal incidence, Kovyakov *et al.*[43] showed that the scattering properties of gratings bounded by a gain layer(s) diverge on resonance when the gain precisely compensates for the loss of the excited SPP. They predicted a transmittance and reflectance of 20 dB for a material gain of

© 2011 Macmillan Publishers Limited. All rights reserved.

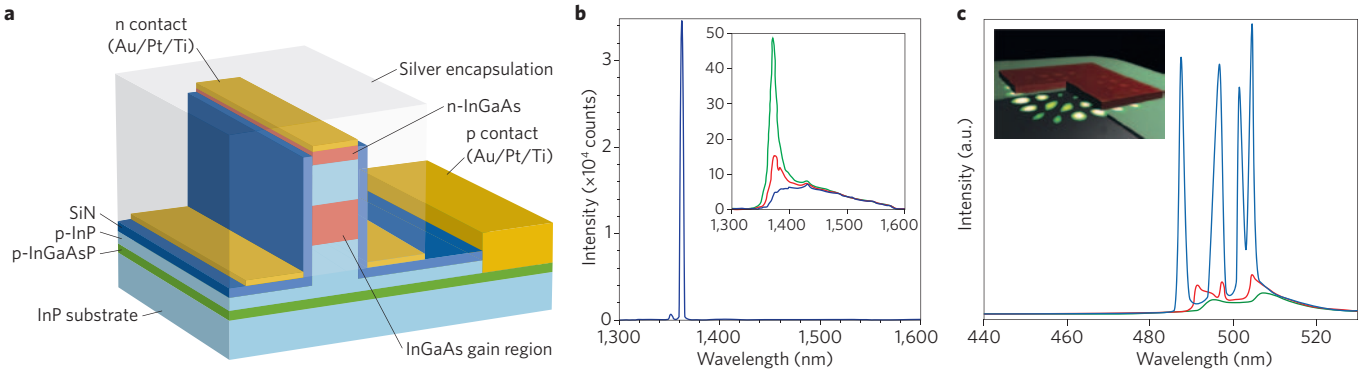

Figure 3 | SPP lasers. a, Fabry–Pérot metal-clad SPP laser comprising an Ag/SiN-coated rectangular InGaAs pillar; the thickness of the InGaAs gain region is 300 nm. **b**, Measured laser spectrum at 10 K for a 6-μm-long device biased at 200 μA; the width of the gain pillar is d = 90 nm and the thickness of the SiN layer is around 20 nm for a total width of approximately 130 nm. The inset shows emission spectra (also at 10 K) below the lasing threshold. **c**, Measured leakage spectra as a function of pump irradiance (black, 1,960 MW cm^{-2}; red, 2,300 MW cm^{-2}; blue, 3,074 MW cm^{-2}). Inset shows an SPP cavity formed from a silver film covered by a 5-nm-thick layer of MgF_2 and a square patch of CdS measuring 50 nm thick and 1 μm across. Figure reproduced with permission from: **a**,**b**, ref. 58, © 2009 OSA; **c**, ref. 73, © 2011 NPG.

4,670 cm^{-1} when the symmetric SPP is resonantly excited, although this assumes that the system will remain stable (that is, SPP oscillation will not occur).

Researchers have reported several experimental studies that involve LRSPP propagation though a gain region, ranging from stimulated emission to demonstrations of amplification and lasing. The stimulated emission of LRSPPs was first observed at λ = 1,532 nm on a gold stripe (20 nm thick and 8 μm wide) embedded in erbium-doped glass in a co-propagating LRSPP pump–probe arrangement[41]. The first measurements of LRSPP amplification were demonstrated by De Leon and Berini[46] using an insertion arrangement (Fig. 2a). The structure consisted of a gold stripe (20 nm thick, 1 μm wide and 2.7 mm long) on SiO_2 covered by 100 μm of IR-140 dye ($N = 6 \times 10^{17}$ cm^{-3}) in a solvent index-matched to SiO_2. The structure was pumped from the top (λ = 808 nm, 20 mJ cm^{-2}, 8 ns pulses) and probed at λ = 882 nm using butt-coupled optical fibres. Gain measurements were obtained as a function of the amplifier length l_a, as shown in Fig. 2b, from which the slope yields an LRSPP mode power gain of γ = 8.55 dB mm^{-1} (around 20 cm^{-1}). In a subsequent study[50], the researchers revealed how the spectrum narrows with increasing pump length for ASE-LRSPPs (Fig. 2b, left inset) and deduced an effective input noise power per unit bandwidth of around 3.3 photons per mode. Details on their measurement techniques were also reported[51]. Gather *et al.*[47] achieved LRSPP amplification at visible wavelengths on a 4-nm-thick gold film covered by a 1-μm-thick polymeric gain layer. The structure was pumped from the top (λ = 532 nm, 5 ns pulses) and ASE-LRSPP measurements were obtained as a function of pump intensity and length. The researchers reported a narrowing of the ASE-LRSPP spectrum, threshold behaviour in the emitted intensity, and an LRSPP mode power gain of around 8 cm^{-1} at $\lambda \approx$ 600 nm. LRSPP lasing (oscillation) was reported by Flynn *et al.*[52] at $\lambda \approx$ 1.46 μm in a symmetric InP-based structure consisting of a 15-nm-thick gold film placed between multiple quantum well stacks providing TM gain. Lasing was observed as TM-polarized light emitted from an end facet of a 1-mm-long, 100-μm-wide Fabry–Pérot cavity while pumping from the top (λ = 1.06 μm, 140 ns pulses).

SPPs in metal-clad waveguides

Symmetric short-range SPPs (SRSPPs) can be confined to very small sizes in metal-gap[53] and metal-clad[54] waveguides, which motivates their use for nano-amplifier and nanolaser applications[55–62]. Although the attenuation of SRSPPs is high, theoretical studies have shown that semiconductors can provide enough gain to compensate for losses in some structures[55–57,59–61]. Maier[55] determined that material gains in the range of 1,625–4,830 cm^{-1} are required for lossless SPP propagation at λ = 1,500 nm for a gold-clad semiconductor film measuring 50–500 nm in thickness. Modelling an Au–InGaAs–Au structure, Chen *et al.*[61] predicted lossless SPP propagation at λ = 1,550 nm for a material gain of 2,500 cm^{-1} in a 75-nm-thick structure. They also investigated the performance of a nanoring laser and predicted a threshold lasing current (density) of around 550 nA (1 kA cm^{-2}). Interestingly, Li and Ning[60] computed that the gain of the SPP near its energy asymptote is much larger than the material gain of the medium clad by metals because the mode energy velocity is low in this region.

Hill *et al.*[58] demonstrated electrically pumped SPP lasing by coating narrow vertical structures formed on rectangular InGaAs pillars with a 20-nm-thick SiN passivation layer followed by a silver layer (Fig. 3a). Strong confinement occurred along the horizontal dimension and index confinement occurred along the vertical dimension. Mirror reflections at the end facets defined a Fabry–Pérot cavity of length l. The laser emission was detected as leakage radiation through the substrate. Figure 3b shows measured spectra at 10 K above and below (inset) the lasing threshold. The structure was 6 μm long and approximately 130 nm wide.

Other planar structures

A thin patterned dielectric layer on a metal film can act to confine or redirect SPPs[63]. Such structures, known as dielectric-loaded SPP (DLSPP) waveguides, have confinement and attenuation levels comparable to those of an SISPP. The dielectric layer is a natural host for dipolar emitters[64–69]; Grandidier *et al.*[64] investigated waveguides consisting of PMMA stripes (cross-section of 600 nm × 400 nm) doped with PbS QDs on a 40-nm-thick gold film. The researchers conducted measurements of spontaneous and stimulated SPPs using Fourier-plane leakage radiation microscopy at $\lambda \approx$ 1,550 nm (near the QD emission peak) while pumping at λ = 532 nm. They measured the SPP propagation length as a function of pump intensity while probing at λ = 1,550 nm, observing a distinct threshold beyond which the propagation length increased linearly (up to 27% in this work) with the pump power. In subsequent work[66], when investigating CdSe/ZnSe QD-doped PMMA stripes on a silver film, the researchers measured a comparable increase in propagation length at λ = 632.8 nm. Radko *et al.*[68] reported a comparable (32%) increase in SPP propagation length in PbS QD-doped PMMA stripes on gold at $\lambda \approx$ 860 nm. By modelling DLSPP waveguides at wavelengths close to the SPP energy asymptote, Rao and Tang[69] found

© 2011 Macmillan Publishers Limited. All rights reserved.

that nanoscale dielectric cross-sections of around 22 nm × 20 nm and dielectric gains of approximately 46,000 cm^{-1} would provide lossless subwavelength propagation at $\lambda = 450$ nm.

A metal surface covered by low- and high-refractive-index dielectric materials supports an SPP with field localization in the low-refractive-index region[70,71]. A semiconductor gain medium can be integrated naturally as the high-refractive-index region, leading to SPP loss compensation and lasing in cases where the SPP overlaps sufficiently with the gain medium. Oulton *et al.*[72] demonstrated laser-like behaviour at cryogenic temperatures in SPPs propagating on a silver film covered by a thin MgF_2 layer supporting a CdS nanowire serving as the gain medium and thus defining a Fabry–Pérot cavity. The researchers also investigated a variant based on a square patch of CdS (ref. 73; Fig. 3c, inset). The patch was pumped using a pulsed femtosecond Ti:sapphire laser. Figure 3c gives room-temperature leakage spectra with increasing pump intensity, showing the onset of lasing in four cavity modes. Single-mode lasing was also observed in an irregularly shaped patch.

Nanostructures

Small metal particles support resonant SPP modes that are characteristic of the particle's shape, size and composition, and also of the surrounding dielectric[74,75]. The fundamental resonant mode of a metal nanosphere, for example, is dipolar, with densities of opposing charge forming at opposite spherical caps. Resonances are excited by an applied laser field or nearby dipolar emitters. On resonance, the electric field in the vicinity of the particle is strongly enhanced (10–100 times) relative to the applied field.

Resonances on metal nanoparticles coupled to a gain medium are of interest because such systems can oscillate and thus act as nanolasers[76–83]. The general concept, proposed by Bergman and Stockman[76], consists of a metal nanoresonator coupled to a gain medium via near-fields. The nanoresonator provides feedback, which, together with the inverted gain medium, forms a structure capable of sustained oscillation. Bergman and Stockman referred to this optical process as surface plasmon amplification by the stimulated emission of radiation (SPASER), and although this term applies to any SPP amplifier or oscillator, it remains closely associated with the original concept of the nanoparticle oscillator. The inset of Fig. 4a shows a dielectric-core/Ag-shell nanoparticle coated with QDs[79]. The nanoparticle supports resonant SPPs that overlap spatially and spectrally with the QDs. The main part of Fig. 4a shows the energy levels and transitions involved in such a situation: an optical pump creates excitons in a QD (black and green vertical arrows), which then recombine by sending their energy into a resonant SPP (red arrows). These recombination events occur with high probability partly because of the large field enhancement associated with the SPPs on the nanoparticle. Oscillation in a linear chain of silver nanospheres surrounded by QDs[77] and in a bowtie resonator with QDs in the gap has also been investigated[80]. Furthermore, researchers have suggested that a spaser could be adapted for use as an ultrafast amplifier or bistable device[83]. Protsenko *et al.* proposed a similar concept referred to as the 'dipole nanolaser'[78] and used a dipole–dipole model to predict that oscillation would occur for one QD coupled to a silver nanosphere. However, this was called into question[83] based on the small dipole separations assumed in the model, and further analysis suggested that the emission would consist of a train of single photons whose individual energy would be within a broad spectral range[81].

The spaser was investigated experimentally by Noginov *et al.*[82], who observed laser-like emission from spherical spaser particles. Such a particle, shown in the inset of Fig. 4b, consisted of a 14 nm gold core coated with a 15 nm SiO_2 shell doped with around 2,700 molecules of Oregon Green 488 dye ($N = 6.25 \times 10^{19}$ cm^{-3}). The dye emission ($\lambda \approx 510$ nm) overlapped well with the broad resonance of the particles ($\lambda \approx 520$ nm). The researchers measured the spectral

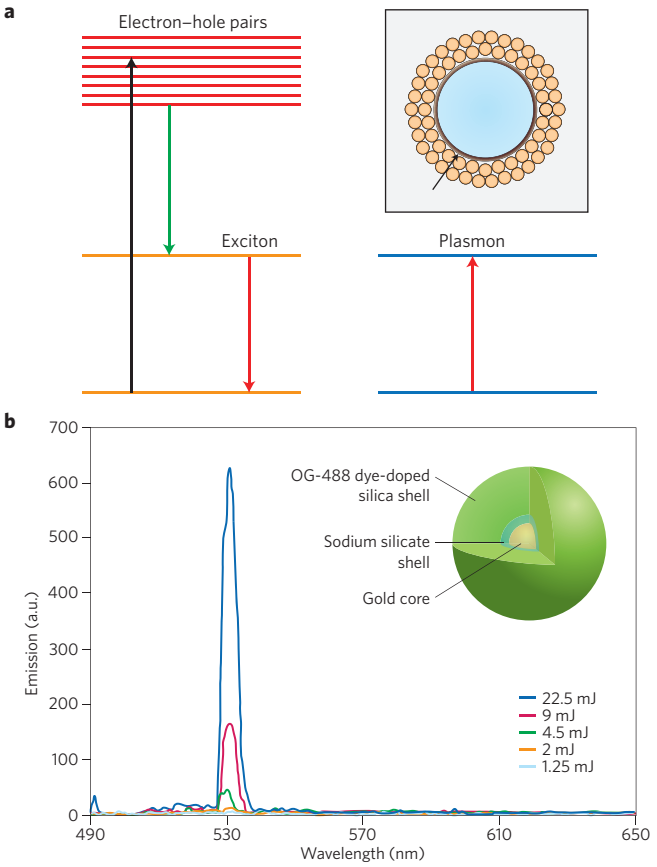

Figure 4 | The spaser. a, The energy levels and transitions of a spaser particle (inset) comprising a dielectric-core/Ag-shell nanoparticle measuring 20–40 nm in diameter and coated with QDs (orange). The thin silver shell is identified by the black arrow. **b**, Emitted spectra of spaser particles as a function of pump energy. Inset, one of the spaser particles under investigation, showing the 14-nm-diameter gold core coated by a 15-nm-thick SiO_2 shell doped with Oregon Green 488 dye molecules. Figure reproduced with permission from: **a**, ref. 79, © 2008 NPG; **b**, ref. 82, © 2009 NPG.

and temporal characteristics of light leaking from the particles suspended in solution when optically pumped ($\lambda = 488$ nm, 5 ns pulses). Figure 4b shows example spectra that peak at $\lambda = 531$ nm; the magnitude of the peak increases linearly with increased pumping, beyond a certain threshold. These results are independent of the particle concentration, which suggests that the spectra originated from individual particles rather than from a collective response. It would be interesting to investigate individual spaser particles (under pumping) using near-field scanning microscopy techniques[1,4].

The scattering properties of metal nanoparticles coupled to a gain medium are also of interest because such systems may lead to enhanced (near-singular) scattering[84–86], which is useful, for example, in Raman sensing[87]. Computations suggest that metallic nanospheres embedded in a medium providing 1,500–2,500 cm^{-1} of gain would produce scattering singularities[84]; similar predictions (but involving higher gains) have been made for core–shell nanoparticles[86]. Although experimental evidence supports enhanced scattering[85], consideration must be given to the stability (non-oscillation) of such systems: a resonant nanoparticle (that is, a feedback element) coupled to a gain medium will oscillate if sufficient gain is provided, which limits the overall achievable scattering enhancement; singularities in scattering parameters indicate the threshold gain for the onset of oscillation.

© 2011 Macmillan Publishers Limited. All rights reserved.

A linear chain of metal nanospheres can be used as a waveguide supporting the transverse or longitudinal propagation (sphere-to-sphere) of polarization associated with SPP resonances[88]. Such propagation is strongly damped, thus prompting the investigation of loss compensation by gain[89–92]. This approach raises concerns regarding the stability of an amplified chain, given that individual nanoparticles sustain resonances.

Cylindrical structures such as metal rods, or dielectric rods clad by a metal sheath, support particular modes whose strong SPP character leads to field localization and an energy asymptote[93]. Studies involving SPP propagation on such structures incorporating gain have been reported[94–97]. Kitur *et al.*[97] observed laser-like emission from gold and silver microwires coated with R6G-doped (21 mM) PMMA, pumped from the side (10 ns, λ = 532 nm); the researchers believed the emission spectra to originate from lasing in SPP whispering gallery modes that circulate along the azimuthal direction on the wires along the metal–PMMA interface. Metal-clad cylindrical microcavities involving hybrid dielectric–SPP modes are also of interest for laser applications[98–100].

Prospects

Structures that provide strong SPP confinement do so with the drawback of high attenuation — adding optical gain to compensate for loss alters this trade-off and thus allows SPPs to propagate over longer distances. In order of increasing confinement, the approximate small-signal material gains required for lossless SPP propagation are: 1–200 cm^{-1} for LRSPPs along thin (around 20 nm) metal films; 1,000–2,000 cm^{-1} for SISPPs; 2,000–5,000 cm^{-1} for SPPs along thin (50 nm) metal-clad waveguides; and 80,000 cm^{-1} for SPPs near their energy asymptote. Resonant SPPs on metal nanospheres can oscillate when embedded in a material with around 3,000 cm^{-1} of gain.

Such levels of gain are available from dyes and semiconductor quantum structures, except perhaps for the very high gains needed for SPPs near their asymptote. For example, 5 mM ($N = 3 \times 10^{18}$ cm^{-3}) of R6G provides 100–500 cm^{-1} of gain at λ = 560 nm, whereas 40 mM of the same dye should provide 2,000–3,500 cm^{-1} (upper limits at full inversion)[45]. 1 mM of IR-140 provides up to 360 cm^{-1} of gain at λ = 880 nm (full inversion)[46]. One strained quantum well ($In_{0.53}Ga_{0.47}As$) provides around 2,000 cm^{-1} of TM gain at λ = 1,500 nm (ref. 101), with significantly higher gains being possible in epitaxial AlAs/GaAs QDs (68,000 cm^{-1} at λ = 970 nm)[102]. The gains available from doped glasses are comparatively smaller due to co-operative upconversion[103]; for example, a maximum of 1 cm^{-1} for heavily doped erbium glass (λ = 1,535 nm).

Optical dipoles (such as dyes) can be incorporated into dielectrics (such as polymers and glasses) and conveniently integrated with metal SPP structures. Unfortunately, there are limits to the gains achievable using such media (see ref. 45 and references therein, for example). Although the solubility limit of dyes may be very high, the concentrations used in practice are far lower because of concentration-dependent effects that limit the excited state population density (such as Förster energy transfer between dipoles) or reduce the quantum efficiency and lifetime of the dipoles (such as the formation of dimers or clusters). High concentrations of dye can also make it difficult for the pump energy to propagate to the surface of the metal, where it is needed. Increasing the pump intensity to produce deeper inversion also has limits because multiphoton processes such as excited state absorption may become significant. Metal features can also be damaged by the pump: one value for the ablation threshold of bulk silver, for example, is around 160 MW cm^{-2} (20 min exposure, 5 ns pulses, 0.8 J cm^{-2}, 0.16 Hz repetition rate, λ = 532 nm)[104], but microscopic thermally induced damage occurs at lower intensities and small features are far more susceptible than bulk metal. Epitaxial semiconductors mitigate many of these problems but can be difficult to integrate with a target plasmonic structure. In addition, the gain in such a material is generally polarization-dependant, which means the material must be correctly aligned with the SPP field.

Several important advances on SPP amplification and lasing have been reported so far, some of which have been described and discussed here. However, much work remains, particularly for the development of applications that demand high performance and usability. There are seven major aspects that require further improvement. (1) Pumping. Although suitable for some applications, optical pumping may be inconvenient and strong optical pumping generates heat and causes damage. Electrical pumping is more convenient than optical pumping but is essentially limited to semiconductors. (2) Resonators. The passive Q of a plasmonic cavity worsens as the SPP confinement increases, leading to a decrease in coherence and broader lasing spectra. (3) Power dissipation. Severe limits on power dissipation exist in applications such as information and communications technologies. (4) Efficiency. The energy efficiency of SPP amplification and lasing must be improved, although gain reduction close to the metal due to dipole quenching may place stringent limits. (5) Signal-to-noise ratio. Noise constrains the information transmission capacity of communications channels. The generation and amplification of noise (spontaneous emission) in SPP amplifiers and lasers must be better understood. (6) Operating temperature. Operation at or near room temperature is necessary for mainstream applications. (7) Stability. The stability of loss-compensating, amplifying or scattering systems must be considered, given that large material gains are involved. High-gain amplifiers are particularly susceptible to instability (oscillation) induced by unexpected reflections that provide unwanted feedback.

Despite these challenges, the prospects for SPP amplifiers and lasers are exciting. Convincing demonstrations of amplification and lasing have already been reported for different kinds of SPPs on diverse metallic structures, including SISPPs on planes[19] and cylinders[97], LRSPPs on stripes[46] and planes[47,52], SPPs in metal-clad waveguides[58] and other planar structures[73], and SPPs on spaser particles[82]. Building on such demonstrations, while paying attention to the issues mentioned above, will lead to useful and hitherto unimagined applications. Given the rapid pace of progress in this emerging and exciting field, such applications may be just around the corner.

References

1. Maier, S. A. *Plasmonics: Fundamentals and Applications* (Springer, 2007).
2. Stiles, P. L., Dieringer, D. J., Shah, N. C. & Van Duyne, R. P. Surface-enhanced Raman spectroscopy. *Ann. Rev. Anal. Chem.* **1,** 601–626 (2008).
3. Barnes, W. L., Dereux, A. & Ebbesen, T. W. Surface plasmon subwavelength optics. *Nature* **424,** 824–830 (2003).
4. Gramotnev, D. K. & Bozhevolnyi, S. I. Plasmonics beyond the diffraction limit. *Nature Photon.* **4,** 83–91 (2010).
5. Kawata, S., Inouye, Y. & Verma, P. Plasmonics for near-field nano-imaging and superlensing. *Nature Photon.* **3,** 388–394 (2009).
6. Anker, J. N. *et al.* Biosensing with plasmonic nanosensors. *Nature Mater.* **7,** 442–453 (2008).
7. Homola, J. Surface plasmon resonance sensors for detection of chemical and biological species. *Chem. Rev.* **108,** 462–493 (2008).
8. Ebbesen, T. W., Genet, C. & Bozhevolnyi, S. I. Surface plasmon circuitry. *Phys. Today* **61,** 44–50 (2008).
9. Palik, E. D. (ed.) *Handbook of Optical Constants of Solids* (Academic, 1985).
10. Arakawa, E. T., Williams, M. W., Hamm, R. N. & Ritchie, R. H. Effect of damping on surface plasmon dispersion. *Phys. Rev. Lett.* **31,** 1127–1129 (1973).
11. Zia, R., Selker, M. D., Catrysse, P. B. & Brongersma, M. L. Geometries and materials for subwavelength surface plasmon modes. *J. Opt. Soc. Am. A* **21,** 2442–2446 (2004).
12. Berini, P. Figures of merit for surface plasmon waveguides. *Opt. Express* **14,** 13030–13042 (2006).
13. Nkoma, J., Loudon, R. & Tilley, D. R. Elementary properties of surface plasmons. *J. Phys. C* **7,** 3547–3559 (1974).
14. Archambault, A., Marquier, F. & Greffet, J.-J. Quantum theory of spontaneous and stimulated emission of surface plasmons. *Phys. Rev. B* **82,** 035411 (2010).
15. Matloob, R., Loudon, R., Barnett, S. M. & Jeffers, J. Electromagnetic field quantization in absorbing dielectrics. *Phys. Rev. A* **52,** 4823–4838 (1995).

© 2011 Macmillan Publishers Limited. All rights reserved.

16. Barnes, W. L. Fluorescence near interfaces: the role of photonic mode density. *J. Mod. Opt.* **45,** 661–669 (1998).
17. Plotz, G., Simon, H. & Tucciarone, J. Enhanced total reflection with surface plasmons. *J. Opt. Soc. Am.* **69,** 419–422 (1979).
18. Sudarkin, A. N. & Demkovich, P. A. Excitation of surface electromagnetic waves on the boundary of a metal with an amplifying medium. *Sov. Phys. Tech. Phys.* **34,** 764–766 (1988).
19. Sirtori, C. *et al.* Long-wavelength ($\lambda \approx 11.5$ μm) semiconductor lasers with waveguides based on surface plasmons. *Opt. Lett.* **23,** 1366–1368 (1998).
20. Tredicucci, A. *et al.* Single-mode surface-plasmon laser. *App. Phys. Lett.* **76,** 2164–2166 (2000).
21. Avrutsky, I. Surface plasmons at nanoscale relief gratings between a metal and a dielectric medium with optical gain. *Phys. Rev. B.* **70,** 155416 (2004).
22. Nezhad, M. P., Tetz, K. & Fainman, Y. Gain assisted propagation of surface plasmon polaritons on planar metallic waveguides. *Opt. Express* **12,** 4072–4079 (2004).
23. Seidel, J., Grafstrom, S. & Eng, L. Stimulated emission of surface plasmons at the interface between a silver film and an optically pumped dye solution. *Phys. Rev. Lett.* **94,** 177401 (2005).
24. Noginov, M. A. *et al.* Compensation of loss in propagating surface plasmon polariton by gain in adjacent dielectric medium. *Opt. Express* **16,** 1385–1392 (2008).
25. Kumar, P., Tripathi, V. K. & Liu, C. S. A surface plasmon laser. *J. Appl. Phys* **104,** 033306 (2008).
26. Noginov, M. A. *et al.* Stimulated emission of surface plasmon polaritons. *Phys. Rev. Lett.* **101,** 226806 (2008).
27. Li, R., Banerjee, A. & Grebel, H. The possibility for surface plasmon lasers. *Opt. Express* **17,** 1622–1627 (2009).
28. Banerjee, A., Li, R. & Grebel, H. Surface plasmon lasers with quantum dots as gain media. *Appl. Phys. Lett.* **95,** 251106 (2009).
29. Bolger, P. M. *et al.* Amplified spontaneous emission of surface plasmon polaritons and limitations on the increase of their propagation length. *Opt. Lett.* **35,** 1197–1199 (2010).
30. Lu, F. F. *et al.* Surface plasmon polariton enhanced by optical parametric amplification in nonlinear hybrid waveguide. *Opt. Express* **19,** 2858–2865 (2011).
31. Kovacs, G. J. Optical excitation of surface plasma waves in an indium film bounded by dielectric layers. *Thin Solid Films* **60,** 33–44 (1979).
32. Fukui, M., So, V. C. Y. & Normandin, R. Lifetimes of surface plasmons in thin silver films. *Phys. Status Solidi B* **91**, K61–K64 (1979).
33. Sarid, D. Long-range surface-plasma waves on very thin metal films. *Phys. Rev. Lett.* **47,** 1927–1930 (1981).
34. Berini, P. Plasmon-polariton waves guided by thin lossy metal films of finite width: bound modes of symmetric structures. *Phys. Rev. B* **61,** 10484–10503 (2000).
35. Okamoto, T., H'Dhili, F. & Kawata, S. Towards plasmonic band gap laser. *Appl. Phys. Lett.* **85,** 3968–3970 (2004).
36. Winter, G., Wedge, S. & Barnes, W. L. Can lasing at visible wavelength be achieved using the low-loss long-range surface plasmon-polariton mode? *New J. Phys.* **8,** 125 (2006).
37. Alam, M. Z., Meier, J., Aitchison, J. S. & Mojahedi, M. Gain assisted surface plasmon polariton in quantum well structures. *Opt. Express* **15,** 176–182 (2007).
38. Genov, D. A., Ambati, M. & Zhang, X. Surface plasmon amplification in planar metal films. *IEEE J. Quant. Electron.* **43,** 1104–1108 (2007).
39. Okamoto, T., Simonen, J. & Kawata, S. Plasmonic band gaps of structured metallic thin films evaluated for a surface plasmon laser using the coupled-wave approach. *Phys. Rev. B* **77,** 115425 (2008).
40. De Leon, I. & Berini, P. Theory of surface plasmon-polariton amplification in planar structures incorporating dipolar gain media. *Phys. Rev. B* **78,** 161401(R) (2008).
41. Ambati, M. *et al.* Observation of stimulated emission of surface plasmon polaritons. *Nano Lett.* **8,** 3998–4001 (2008).
42. Ambati, M., Genov, D. A., Oulton, R. F. & Zhang, X. Active plasmonics: surface plasmon interaction with optical emitters. *IEEE J. Sel. Top. Quant. Electron.* **14,** 1395–1403 (2008).
43. Kovyakov, A., Zakharian, A. R., Gundu, K. M. & Darmanyan, S. A. Giant optical resonances due to gain-assisted Bloch surface plasmon. *Appl. Phys. Lett.* **94,** 151111 (2009).
44. Berini, P. Long-range surface plasmon polaritons. *Adv. Opt. Photon.* **1,** 484–588 (2009).
45. De Leon, I. & Berini, P. Modeling surface plasmon-polariton gain in planar metallic structures. *Opt. Express* **17,** 20191–20202 (2009).
46. De Leon, I. & Berini, P. Amplification of long-range surface plasmons by a dipolar gain medium. *Nature Photon.* **4,** 382–387 (2010).
47. Gather, M. C., Meerholz, K., Danz, N. & Leosson K. Net optical gain in a plasmonic waveguide embedded in a fluorescent polymer. *Nature Photon.* **4,** 457–461 (2010).
48. H'Dhili, F., Okamoto, T., Simonen, J. & Kawata, S. Improving the emission efficiency of periodic plasmonic structures for lasing applications. *Opt. Comm.* **284,** 561–566 (2011).
49. Chen, Y.-H. & Guo, L. J. High *Q* long-range surface plasmon polariton modes in sub-wavelength metallic microdisk cavity. *Plasmonics* **6,** 183–188 (2011).
50. De Leon, I. & Berini, P. Spontaneous emission in long-range surface plasmon-polariton amplifiers. *Phys. Rev. B* **83,** 081414(R) (2011).
51. De Leon, I. & Berini, P. Measuring gain and noise in active long-range surface plasmon-polariton waveguides. *Rev. Sci. Instr.* **82,** 033107 (2011).
52. Flynn, R. A. *et al.* A room-temperature semiconductor spaser operating near 1.5 μm. *Opt. Express* **19,** 8954–8961 (2011).
53. Pile, D. F. P. *et al.* Two-dimensionally localized modes of a nanoscale gap plasmon waveguide. *Appl. Phys. Lett.* **87,** 261114 (2005).
54. Dionne, J. A, Sweatlock, L. A., Atwater, H. A. & Polman A. Plasmon slot waveguides: towards chip-scale propagation with subwavelength-scale localization. *Phys. Rev. B* **73,** 035407 (2006).
55. Maier, S. A. Gain-assisted propagation of electromagnetic energy in sub-wavelength surface plasmon polariton gap waveguides. *Opt. Comm.* **258,** 295–299 (2006).
56. Yu, Z., Veronis, G., Fan, S. & Brongersma, M. L. Gain-induced switching in metal-dielectric-metal plasmonic waveguides. *Appl. Phys. Lett.* **92,** 041117 (2008).
57. Chang, S.-W. & Chuang, S. L. Normal modes for plasmonic nanolasers with dispersive and inhomogeneous media. *Opt. Lett.* **34,** 91–93 (2009).
58. Hill, M. T. *et al.* Lasing in metal-insulator-metal sub-wavelength plasmonic waveguides. *Opt. Express* **17,** 11107–11112 (2009).
59. Chang, S.-W. & Chuang, S. L. Fundamental formulation for plasmonic nanolasers. *IEEE J. Quant. Electron.* **45,** 1014–1023 (2009).
60. Li, D. B. & Ning, C. Z. Giant modal gain, amplified surface plasmon-polariton propagation, and slowing down of energy velocity in a metal-semiconductor-metal structure. *Phys. Rev. B* **80,** 153304 (2009).
61. Chen, X., Bhola, B., Huang, Y. & Ho, S. T. Multi-level multi-thermal-electron FDTD simulation of plasmonic interaction with semiconducting gain media: applications to plasmonic amplifiers and nano-lasers. *Opt. Express* **18,** 17220–17238 (2010).
62. Hill, M. T. Status and prospects for metallic and plasmonic nano-lasers. *J. Opt. Soc. Am. B* **27**, B36–B44 (2010).
63. Hohenau, A. *et al.* Dielectric optical elements for surface plasmons. *Opt. Lett.* **30,** 892–895 (2005).
64. Grandidier, J. *et al.* Gain-assisted propagation in a plasmonic waveguide at telecom wavelength. *Nano Lett.* **9,** 2935–2939 (2009).
65. Krishnan, A., Frisbie, S. P., Grave de Peralta, L. & Bernussi, A. A. Plasmon stimulated emission in arrays of bimetallic structures coated with dye-doped dielectric. *Appl. Phys. Lett.* **96,** 111104 (2010).
66. Grandidier, J. *et al.* Leakage radiation microscopy of surface plasmon coupled emission: investigation of gain-assisted propagation in an integrated plasmonic waveguide. *J. Microscopy* **239,** 167–172 (2010).
67. Colas Des Francs, G. *et al.* Optical gain, spontaneous and stimulated emission of surface plasmon polaritons in confined plasmonic waveguide. *Opt. Express* **18,** 16327–16334 (2010).
68. Radko, I. P., Nielsen, M. G., Albrektsen, O. & Bozhevolnyi, S. I. Stimulated emission of surface plasmon polaritons by lead-sulfide quantum dots at near infra-red wavelengths. *Opt. Express* **18,** 18633–18641 (2010).
69. Rao, R. & Tang, T. Study on active surface plasmon waveguides and design of a nanoscale lossless surface plasmon waveguide. *J. Opt. Soc. Am. B* **28,** 1258–1265 (2011).
70. Alam, M. Z., Meier, J., Aitchison, J. S. & Mojahedi, M. Super mode propagation in low index medium. *Proc. CLEO* paper JThD112 (2007).
71. Oulton, R. F., Sorger, V. J., Genov, D. A., Pile, D. F. P. & Zhang, X. A hybrid plasmonic waveguide for subwavelength confinement and long-range propagation. *Nature Photon.* **2,** 496–500 (2008).
72. Oulton, R. F. *et al.* Plasmon lasers at deep subwavelength scale. *Nature* **461,** 629–632 (2009).
73. Ma, R.-M., Oulton, R. F., Sorger, V. J., Bartal, G. & Zhang, X. Room-temperature sub-diffraction-limited plasmon laser by total internal reflection. *Nature Mater.* **10,** 110–113 (2011).
74. Kelly, K. L., Coronado, E., Zhao, L. L. & Schatz, G. C. The optical properties of metal nanoparticles: the influence of size, shape, and dielectric environment. *J. Phys. Chem. B* **107,** 668–677 (2003).
75. Pelton, M., Aizpurua, J. & Bryant, G. Metal-nanoparticle plasmonics. *Laser Photon. Rev.* **2,** 136–159 (2008).
76. Bergman, D. J. & Stockman, M. I. Surface plasmon amplification by stimulated emission of radiation: quantum generation of coherent surface plasmons in nanosystems. *Phys. Rev. Lett.* **90,** 027402 (2003).
77. Li, K., Li, X., Stockman, M. I. & Bergman, D. J. Surface plasmon amplification by stimulated emission in nanolenses. *Phys. Rev. B* **71,** 115409 (2005).

© 2011 Macmillan Publishers Limited. All rights reserved.

78. Protsenko, I. E., Uskov, A. V., Zaimidoroga, O. A., Samoilov, V. N. & O'Reilly, E. P. Dipole nanolaser. *Phys. Rev. A* **71,** 063812 (2005).
79. Stockman, M. I. Spasers explained. *Nature Photon.* **2,** 327–329 (2008).
80. Chang, S.-W., Ni, C.-Y. A. & Chuang, S. L. Theory for bowtie plasmonic nanolasers. *Opt. Express* **16,** 10580–10595 (2008).
81. Rosenthal, A. S. & Ghannam, T. Dipole nanolasers: a study of their quantum properties. *Phys. Rev. A* **79,** 043824 (2009).
82. Noginov, M. A. *et al.* Demonstration of a spaser-based nanolaser. *Nature* **460,** 1110–1113 (2009).
83. Stockman, M. I. The spaser as a nanoscale quantum generator and ultrafast amplifier. *J. Opt.* **12,** 024004 (2010).
84. Lawandy, N. M. Localized surface plasmon singularities in amplifying media. *Appl. Phys. Lett.* **85,** 5040–5042 (2004).
85. Noginov. *et al.* Enhancement of surface plasmons in an Ag aggregate by optical gain in a dielectric medium. *Opt. Lett.* **31,** 3022–3024 (2006).
86. Gordon, J. A. & Ziolkowski, R. W. The design and simulated performance of a coated nano-particle laser. *Opt. Express* **15,** 2622–2653 (2007).
87. Li, Z.-Y. & Xia, Y. Metal nanoparticles with gain toward single-molecule detection by surface-enhanced Raman scattering. *Nano Lett.* **10,** 243–249 (2010).
88. Quinten, M., Leitner, A., Krenn, J. R. & Aussenegg, F. R. Electromagnetic energy transport via linear chains of silver nanoparticles. *Opt. Lett.* **23,** 1331–1333 (1998).
89. Citrin, D. S. Plasmon-polariton transport in metal-nanoparticle chains embedded in a gain medium. *Opt. Lett.* **31,** 98–100 (2006).
90. Thylén, L. *et al.* Limits on integration as determined by power dissipation and signal-to-noise ratio in loss-compensated photonic integrated circuits based on metal/quantum-dot materials. *IEEE J. Quant. Electron.* **46,** 518–524 (2010).
91. Holmström, P., Thylén, L. & Bratkovsky, A. Composite metal/quantum-dot nanoparticle-array waveguides with compensated loss. *Appl. Phys. Lett.* **97,** 073110 (2010).
92. Zhang, H. & Ho, H.-P. Low-loss plasmonic waveguide based on gain-assisted periodic metal mesosphere chains. *Opt. Express* **18,** 23035–23040 (2010).
93. Novotny, L. & Hafner, C. Light propagation in a cylindrical waveguide with a complex metallic dielectric function. *Phys. Rev. E* **50,** 4094–4106 (1994).
94. Govyadinov, A. A. & Podolskiy, V. A. Gain-assisted slow to superluminal group velocity manipulation in nanowaveguides. *Phys. Rev. Lett.* **97,** 223902 (2006).
95. Yang, Z.-J. *et al.* Surface plasmons amplifications in single Ag nanoring. *Opt. Express* **18,** 4006–4011 (2010).
96. Handapangoda, D., Rukhlenko, I. D., Premaratne, M. & Jagadish, C. Optimization of gain-assisted waveguiding in metal-dielectric nanowires. *Opt. Lett.* **35,** 4190–4192 (2010).
97. Kitur, J. K., Podolskiy, V. A. & Noginov, M. A. Stimulated emission of surface plasmon polaritons in a microcylinder cavity. *Phys. Rev. Lett.* **106,** 183903 (2011).
98. Hill, M. T. *et al.* Lasing in metallic-coated nanocavities. *Nature Photon.* **1,** 589–594 (2007).
99. Nezhad, M. P. *et al.* Room-temperature subwavelength metallo-dielectric lasers. *Nature Photon.* **4,** 395–399 (2010).
100. Chang, S.-W., Lin, T.-R. & Chuang, S. L. Theory of plasmonic Fabry–Pérot nanolasers. *Opt. Express* **18,** 15039–15053 (2010).
101. Coldren, L. A. & Corzine, S. W. *Diode lasers and photonic integrated circuits* (Wiley, 1995).
102. Kirstaedter, N. *et al.* Gain and differential gain of single layer InAs/GaAs quantum dot injection lasers. *Appl. Phys. Lett.* **69,** 1226–1228 (1996).
103. Yan, Y. C. *et al.* Erbium-doped phosphate glass waveguide on silicon with 4.1 dB/cm gain at 1.535 μm. *Appl. Phys. Lett.* **71,** 2922–2924 (1997).
104. Svendsen, W., Ellegaard, O. & Schou, J. Laser ablation deposition measurements from silver and nickel. *Appl. Phys. A* **63,** 247–255 (1996).

Acknowledgements

P.B. and I.D.L. acknowledge financial support from the Natural Sciences and Engineering Research Council (NSERC) of Canada.

© 2011 Macmillan Publishers Limited. All rights reserved.